Journal of Visualized Experiments

Recording network activity in spinal nociceptive circuits using microelectrode arrays

--Manuscript Draft--

Article Type:	Invited Methods Collection - JoVE Produced Video
Manuscript Number:	JoVE62920R1
Full Title:	Recording network activity in spinal nociceptive circuits using microelectrode arrays
Corresponding Author:	Brett Graham University of Newcastle Callgahan, NSW AUSTRALIA
Corresponding Author's Institution:	University of Newcastle
Corresponding Author E-Mail:	brett.graham@newcastle.edu.au
Order of Authors:	Jacqueline Iredale
	Jeremy Stoddard
	Hannah Drury
	Tyler Browne
	Augustus Elton
	Jessica Madden
	Robert Callister
	James Welsh
	Brett Graham
Additional Information:	
Question	**Response**
Please specify the section of the submitted manuscript.	Neuroscience
Please indicate whether this article will be Standard Access or Open Access.	Standard Access ($1400)
Please indicate the **city, state/province, and country** where this article will be **filmed**. Please do not use abbreviations.	Callaghan, NSW, Australia
Please confirm that you have read and agree to the terms and conditions of the author license agreement that applies below:	I agree to the Author License Agreement
Please provide any comments to the journal here.	
Please confirm that you have read and agree to the terms and conditions of the video release that applies below:	I agree to the Video Release

Powered by Editorial Manager® and ProduXion Manager® from Aries Systems Corporation

Manuscript Click here to access/download;Manuscript;62920_R1.docx

TITLE:

Recording Network Activity in Spinal Nociceptive Circuits Using Microelectrode Arrays

AUTHORS AND AFFILIATIONS:

Jacqueline A Iredale[1], Jeremy G Stoddard[2], Hannah R Drury[1], Tyler J Browne[1], Augustus Elton[2], Jessica F Madden[1], Robert J Callister[1], James S Welsh[2], Brett A Graham[1]

[1]School of Biomedical Sciences and Pharmacy, University of Newcastle, Callaghan, NSW, Australia; and Hunter Medical Research Institute, New Lambton, NSW, Australia

[2]School of Electrical Engineering, University of Newcastle, Callaghan, NSW, Australia

Email addresses of co-authors:

Jacqueline A Iredale	(jacqueline.iredale@uon.edu.au)
Jeremy G Stoddard	(jeremy.stoddard@uon.edu.au)
Hannah R Drury	(hannah.drury@newcastle.edu.au)
Tyler J Browne	(tyler.browne@uon.edu.au)
Augustus Elton	(augustus.elton@newcastle.edu.au)
Jessica F Madden	(jessica.madden@uon.edu.au)
Robert J Callister	(robert.callister@newcastle.edu.au)
James S Welsh	(james.welsh@newcastle.edu.au)

Corresponding author:

Brett A Graham (brett.graham@newcastle.edu.au)

SUMMARY:

The combined use of microelectrode array technology and 4-aminopyridine-induced chemical stimulation for investigating network-level nociceptive activity in the spinal cord dorsal horn is outlined.

ABSTRACT:

The roles and connectivity of specific types of neurons within the spinal cord dorsal horn (DH) are being delineated at a rapid rate to provide an increasingly detailed view of the circuits underpinning spinal pain processing. However, the effects of these connections for broader network activity in the DH remain less well understood because most studies focus on the activity of single neurons and small microcircuits. Alternatively, the use of microelectrode arrays (MEAs), which can monitor electrical activity across many cells, provides high spatial and temporal resolution of neural activity. Here, the use of MEAs with mouse spinal cord slices to study DH activity induced by chemically stimulating DH circuits with 4-aminopyridine (4-AP) is described. The resulting rhythmic activity is restricted to the superficial DH—stable over time, blocked by tetrodotoxin, and can be investigated in different slice orientations. Together, this preparation provides a platform to investigate DH circuit activity in tissue from naïve animals, animal models of chronic pain, and mice with genetically altered nociceptive function. Furthermore, MEA recordings in 4-AP-stimulated spinal cord slices can be used as a rapid screening tool to assess the capacity of novel antinociceptive compounds to disrupt activity in the spinal cord DH.

INTRODUCTION:

The roles of specific types of inhibitory and excitatory interneurons within the spinal cord DH are being uncovered at a rapid rate[1-4]. Together, interneurons make up over 95% of the neurons in the DH and are involved in sensory processing, including nociception. Furthermore, these interneuron circuits are important for determining whether peripheral signals ascend the neuroaxis to reach the brain and contribute to the perception of pain[5-7]. To date, most studies have investigated the role of DH neurons at either the single-cell or whole-organism level of analysis using combinations of *in vitro* intracellular electrophysiology, neuroanatomical labeling, and *in vivo* behavioral analysis[1,3,8-14]. These approaches have significantly advanced the understanding of the role of specific neuron populations in pain processing. However, a gap remains in understanding how specific cell types and small microcircuits influence large populations of neurons at a microcircuit level to subsequently shape the output of the DH, behavioral responses, and the pain experience.

One technology that can investigate macro-circuit or multicellular-level function is the microelectrode array (MEA)[15,16]. MEAs have been used to investigate nervous system function for several decades[17,18]. In the brain, they have facilitated the study of neuronal development, synaptic plasticity, pharmacological screening, and toxicity testing[17,18]. They can be used for both *in vitro* and *in vivo* applications, depending on the type of MEA. Furthermore, the development of MEAs has evolved rapidly, with different electrode numbers and configurations now available[19]. A key advantage of MEAs is their capacity to simultaneously assess electrical activity in many neurons with high spatial and temporal accuracy via multiple electrodes[15,16]. This provides a broader readout of how neurons interact in circuits and networks, under control conditions and in the presence of locally applied compounds.

One challenge of *in vitro* DH preparations is that ongoing activity levels are typically low. Here, this challenge is addressed in spinal cord DH circuits using the voltage-gated K^+ channel blocker, 4-aminopryidine (4-AP), to chemically stimulate DH circuits. This drug has previously been used to establish rhythmic synchronous electrical activity in the DH of acute spinal cord slices and under acute *in vivo* conditions[20-24]. These experiments have used single-cell patch and extracellular recording or calcium imaging to characterize 4-AP-induced activity[20-25]. Together, this work has demonstrated the requirement of excitatory and inhibitory synaptic transmission and electrical synapses for rhythmic 4-AP-induced activity. Thus, the 4-AP response has been viewed as an approach that unmasks native polysynaptic DH circuits with biological relevance rather than as a drug-induced epiphenomenon. Furthermore, 4-AP-induced activity exhibits a similar response profile to analgesic and antiepileptic drugs as neuropathic pain conditions and has been used to propose novel spinally-based analgesic drug targets such as connexins[20-22].

Here, a preparation that combines MEAs and chemical activation of the spinal DH with 4-AP to study this nociceptive circuitry at the macro-circuit, or network level of analysis, is described. This approach provides a stable and reproducible platform for investigating nociceptive circuits under naive and neuropathic 'pain-like' conditions. This preparation is also readily applicable to test the circuit-level action of known analgesics and to screen novel analgesics in the hyperactive spinal

cord.

PROTOCOL:

Studies were carried out on male and female c57Bl/6 mice aged 3–12 months. All experimental procedures were performed in accordance with the University of Newcastle's Animal Care and Ethics Committee (protocols A-2013-312, and A-2020-002).

1. In vitro electrophysiology

1.1. Preparation of solutions for spinal cord slice preparation and recording

1.1.1. Artificial cerebrospinal fluid

NOTE: Artificial cerebrospinal fluid (aCSF) is used in an interface incubation chamber, where slices are stored until recording commences and during experiments as both perfusate and diluent for drugs. See **Table 1** for the detailed composition.

[Place **Table 1** here]

1.1.1.1. Prepare aCSF containing (in mM) 118 NaCl, 25 $NaHCO_3$, 10 glucose, 2.5 KCl, 1 NaH_2PO_4, 1 $MgCl_2$, and 2.5 $CaCl_2$ by adding the required quantities of the above, excluding $CaCl_2$, to 2 L of distilled water.

1.1.1.2. Bubble the above solution with carbogen (95% O_2, 5% CO_2) for 5 min and add $CaCl_2$.

NOTE: This step prevents $CaCl_2$ precipitation, i.e., the solution should not turn cloudy. For drug application during experiments, dilute the drug stock solutions in aCSF to desired final concentrations.

1.1.2. Sucrose-substituted artificial cerebrospinal fluid

NOTE: Sucrose-substituted aCSF is used during dissection and spinal cord slicing. As indicated by the name, sucrose is substituted for NaCl to reduce neuronal excitation during these procedures while maintaining osmolarity. See **Table 1** for the detailed composition.

1.1.2.1. Prepare sucrose-substituted aCSF containing (in mM) 250 sucrose, 25 $NaHCO_3$, 10 glucose, 2.5 KCl, 1 NaH_2PO_4, 1 $MgCl_2$, and 2.5 $CaCl_2$ by adding the required quantities of all of the above, excluding $CaCl_2$, to 300 mL of distilled water.

1.1.2.2. Bubble the solution with carbogen for 5 min and then add $CaCl_2$.

1.1.2.3. Store the solution in a -80 °C freezer for approximately 40 min or until the solution forms a slurry. Avoid freezing solid and use while in slurry consistency.

1.2. Microelectrode array preparation

NOTE: The contact surface of the MEA requires a pretreatment to make it hydrophilic.

1.2.1. Before the experiment, fill the MEA well with either fetal bovine serum (FBS) or horse serum (HS) for 30 min.

1.2.2. Remove the FBS or HS and thoroughly rinse MEA with approximately five washes of distilled water until the distilled water is no longer foamy. Fill the well with aCSF, ready for use.

1.3. Acute spinal cord slice preparation

NOTE: The mouse spinal cord slice preparation is as previously described by Smith et al.[2]. Ideally, removal of the lumbosacral enlargement should take no more than 8–10 min (steps 1.3.2–1.3.11 below).

1.3.1. Deeply anesthetize the mouse with 100 mg/kg ketamine (i.p.) and then decapitate it using large surgical scissors.

1.3.2. Remove the skin over the abdominal region by making a small cut in the skin at the level of the hips. Pull the skin on either side of the cut rostrally until all the skin is removed, i.e., from the top of the rib cage to the top of the pelvis (both ventrally and dorsally).

1.3.3. Place the body on ice and use a ventral approach to expose the vertebral column by removing all the viscera and cutting through the ribs lateral to the sternum.

1.3.4. Remove the ventral rib cage, both scapulae (cut off at approximately T2), and the lower limbs and pelvis (cut off at approximately the top of the sacrum).

1.3.5. Transfer the vertebral column and rib preparation to a dissecting bath containing ice-cold sucrose aCSF. Pin all four corners of the preparation (ventral surface upwards) by placing pins through the lower back muscles and the attached upper ribs.

1.3.6. Remove all muscle and connective tissue overlying the ventral surface of the vertebrae with rongeurs and identify the vertebral region over the lumbosacral enlargement, which lies approximately beneath the T12 to L2 vertebral bodies.

1.3.7. Remove a vertebral body that is caudal to the lumbosacral enlargement region to provide access to the spinal cord as it sits in the vertebral canal.

1.3.8. Using curved spring scissors, cut through the vertebral pedicles bilaterally while lifting and pulling the vertebral body rostrally to separate the ventral and dorsal aspects of the vertebrae and expose the spinal cord.

1.3.9. Once the vertebral bodies are removed to reveal the lumbosacral enlargement, carefully clear the remaining roots that anchor the spinal cord with spring scissors until the cord floats free.

1.3.10. Isolate the spinal cord with rostral and caudal cuts well above and below the lumbosacral enlargement, allowing the target region of the cord to 'float free.'

NOTE: The preferred slice orientation will determine how the cord is subsequently mounted for sectioning (**Figure 1**).

1.3.11. For transverse slices, lift the lumbosacral segment by an attached root and place it on a pre-cut polystyrene (Styrofoam) block (1 cm x 1 cm x 1 cm) with a shallow channel cut in the center. Use cyanoacrylate adhesive (see the **Table of Materials**) to attach the block and cord to the sectioning platform and place it in the cutting bath containing ice-cold sucrose aCSF (slurry).

NOTE: The shallow channel helps secure and orient the spinal cord, with the dorsal side exposed and the thoracic end of the cord at the bottom of the block.

1.3.12. For sagittal slices, lay a thin line of cyanoacrylate adhesive on the sectioning platform, lift the lumbosacral enlargement by an attached root, and place the cord along the line of glue, ensuring one lateral surface is in the adhesive and the other faces upwards. Place it in the cutting bath containing ice-cold sucrose aCSF (slurry).

1.3.13. For horizontal slices, put a thin line of cyanoacrylate adhesive on the sectioning platform. Lift the lumbosacral enlargement by an attached root, and place the lumbosacral enlargement along the line of adhesive, ensuring the ventral surface is in the adhesive and the dorsal surface faces upwards. Use attached roots to position the cord. Place it in the cutting bath containing ice-cold sucrose aCSF (slurry).

[Place **Figure 1** here]

1.3.14. Obtain 300 µm thick slices (L1-L5, same thickness regardless of orientation) using a vibrating microtome with the following settings: speed 0.06 mm/s, amplitude 2.50 mm, and calibrated to within ±0.02 height amplitude deviation.

1.3.15. Transfer the slices to an air interface incubation chamber containing oxygenated aCSF.

1.3.16. Before recording, allow the slices to equilibrate for 1 h at room temperature (20–24 °C).

1.4. *Microelectrode array recordings*

NOTE: The following steps detail how to use record data from MEA-based experiments on spinal cord slices. Several MEA designs can be used depending on the experiment. Design details for MEAs used in these experiments are shown in **Table 2** and **Figure 2**. Detailed design information has been published by Egert et al.[26] and Thiebaud et al.[27] for planar and 3-dimensional (3D) MEAs, respectively. Both MEA types are composed of 60 titanium nitride electrodes, with a silicon nitride insulating layer and titanium nitride tracks and contact pads.

1.4.1. Experimental setup

1.4.1.1. Turn on the computer and interface board, and start the recording software.

1.4.1.2. Load the pre-assembled recording template (**Figure 3A**). Name the files for the day in the recorder tab.

1.4.1.3. Continuously bubble aCSF with carbogen (5% CO_2, 95% O_2) for the duration of the experiment.

1.4.1.4. Turn the perfusion system on, which is controlled by a peristaltic pump. Place the inlet line into aCSF and the inlet end in a waste beaker. Prime the perfusion lines with aCSF.

1.4.1.5. Prepare 4-AP and any other drug solutions by diluting stocks in 50 mL of aCSF to the required final concentration (e.g., 200 µM for 4-AP).

1.4.1.6. Place the drug solutions in drug pots and bubble them with carbogen.

1.4.2. 4-AP activity

1.4.2.1. Following incubation, transfer a single slice from the incubator using a large-tip Pasteur pipette filled with aCSF.

1.4.2.2. Place the slice in the MEA well and add additional aCSF.

1.4.2.3. Position the slice over the 60-electrode recording array using a fine short hair paintbrush. Avoid contacting the electrodes with the paintbrush or dragging the tissue across the electrodes, especially if using 3D arrays.

NOTE: Depending on the MEA layout, this can be done with or without the assistance of a microscope for accurate positioning.

1.4.2.4. After positioning the slice, place a weighted net over the tissue to hold it in place and promote good contact with MEA electrodes.

NOTE: The slice may need repositioning following net placement.

1.4.2.5. Place the MEA in the recording headstage **(Figure 2A,B)**.

1.4.2.6. Check the position of the tissue over the electrodes using an inverted microscope (2x magnification) to confirm that as many electrodes as possible are under the superficial DH (SDH). Ensure that at least 2–6 electrodes do **not** contact the slice as these electrodes are important for subtracting noise and recording artefacts during analysis **(Figure 2E)**.

1.4.2.7. Turn on the camera, connect it to the device, and take a reference image of the slice relative to the MEA for use during analysis.

1.4.2.8. Press **Start DAQ** in the recording software, and confirm that all electrodes are receiving a clear signal.

NOTE: If the signal is noisy, unclip the headstage, and clean both the MEA contact pads and gold spring contacts with 70% ethanol (use a laboratory wipe to ensure that the pads and contacts are dry after cleaning). If the signal is still noisy, turn off the malfunctioning electrodes in the recording software or note down for exclusion later during analysis.

1.4.2.9. Attach the perfusion inlet and outlet lines to the MEA-well (previously filled with aCSF) and turn the perfusion system on. Check the flow rate, ideally 4–6 bath volumes per minute, and ensure that the outflow is sufficient to prevent overflow of the superfusate.

1.4.2.10. Allow the tissue to equilibrate for 5 min and then record 5 min of raw, unfiltered baseline data.

1.4.2.11. Move the perfusion inlet line from aCSF to a 4-AP solution and wait for 12 min for the 4-AP-induced rhythmic activity to reach steady state (2 min for drugs to reach the bath and 10 min for the activity to peak and then plateau).

1.4.2.12. Record 5 min of 4-AP-induced activity. Be prepared for subsequent recordings to test the drugs or to check the stability of 4-AP.

[Place **Table 2** and **Figure 2** here]

1.4.3. Changing slices

1.4.3.1. Following each recording session, rinse the lines with aCSF.

1.4.3.2. Remove the MEA from the headstage.

1.4.3.3. Remove the net and the tissue from the MEA well, rinse them well with aCSF, and repeat the above steps with a new slice.

2. Data processing and analysis

NOTE: The following steps detail how to use the analysis software for MEA experiments on spinal cord slices. One of the 60 electrodes serves as an internal reference (marked by a trapezoid in **Figure 2 C,D**), while between four and twenty-five of the remaining 59 are positioned under the SDH in an adult mouse spinal cord slice. Subsequent analysis detects extracellular action potential (EAP) and local field potential (LFP) waveforms (see **Figure 3B** for examples) from the raw signal in this region.

2.1. Raw data processing

2.1.1. Open the analysis software and load the pre-made analysis layout (**Figure 3B**).

2.1.2. Open the file of interest and deselect the reference electrode (electrode 15 in 8 x 8 MEA-or electrode E1 in 6 x 10 MEA-configuration) and any electrodes deemed to be excessively noisy.

2.1.3. Set the time window for analysis (0:00 → 5:00 min).

2.1.4. Move to the **Cross-channel filter** tab. Select **Complex reference** and select the **Reference Electrodes** based on the image taken and notes made during the experiment (i.e., those electrodes not under tissue). To apply and check this, press **Explore** before continuing.

2.1.5. Move to the **EAP filter** tab and apply a 2nd order high pass Butterworth filter (200 Hz cut off) to remove LFP activity.

2.1.6. Move to the **LFP filter** tab and apply a 2nd order band pass Butterworth filter (delta frequencies of 0.5-4 Hz) to remove EAP activity.

2.1.7. Move to the **EAP detector** tab and select **Auto threshold**. Tick **Rising** and **Falling edge** boxes and set the **Dead time** to 0.5 ms.

2.1.8. Set **Positive** and **Negative thresholds** based on the data. Inspect the data by returning to the **Raw data analyzer** screen, moving the time marker, and then returning to the **EAP detector** tab and pressing **Explore**. Repeat until satisfied that the set detection threshold is capturing EAPs without capturing noise/non-physiological activity. Use the reference electrodes to identify noise/non-physiological activity.

NOTE: It is necessary to ensure a minimal number of EAPs are detected in reference electrodes where physiological activity will not be occurring. However, rather slight deviations in baseline might be falsely detected as EAPs. This is while still aiming to maximize the number of real events detected in the active electrodes.

2.1.9. Move to the **LFP detector** tab, select the **Manual threshold**, tick **Rising** and **Falling edge** boxes, and set the **Dead time** to 3 ms.

2.1.10. Repeat step 2.1.8 for one electrode by selecting an electrode with LFP activity. Once satisfied, select **Apply to all** as thresholds will only be applied to a single electrode when undertaking manual thresholding.

2.1.11. While examining LFP data in the **Detector** tab, note the maximum number of threshold crossings for the one LFP waveform and maximum time separation of threshold crossings for the one LFP waveform for use in later analysis.

2.1.12. Press **Start analysis**.

2.1.13. When the analysis is complete, move to the **EAP analyzer** tab and export the data. Do the same on the **LFP analyzer** tab.

2.1.14. Repeat this process for all other files from the same slice.

2.1.15. Following data export, convert the files to xlsx format so they can be read by the programming script used. Name the files according to the following convention for the provided script to read them: experiment name (e.g., sample data) – slice number (e.g., S1) – recording number (e.g., R1) – activity type (e.g., spikes or SPs, corresponding to EAPs or LFPs, respectively).

NOTE: The EAP analysis described here treats spiking from individual channels as a single population, even though this activity would commonly arise from multiple neurons in close proximity to the recording electrode. If the number of neurons contributing to EAPs in a channel is desired, multispike sorting techniques described elsewhere can be applied to distinguish distinct populations of spikes based on waveform characteristics[28].

[Place **Figure 3** here]

2.2. Synchronicity analysis

NOTE: Synchronicity, or the number of 'coincident' events between two electrodes, was determined using the coincidence criterion within the A-SPIKE-synchronization method outlined by Satuvuori *et al.*[29]. The script used here only compares electrodes adjacent to one another for efficiency (i.e., horizontal, vertical, and diagonal neighbors); however, the script could be rewritten to compare all electrodes if required.

2.2.1. Perform data analysis using a custom programming script, which extracts latency timestamps for each electrode from the .xlsx files.

NOTE: This can be done manually.

2.2.2. In step 2.1.10, record the maximum number of threshold crossings and maximum time separation of threshold crossings for the one LFP waveform. Modify the script for inputting these LFP-defining parameters for each slice before running the script.

NOTE: Thresholding previously performed in analysis software clearly captures EAPs as a single event. However, LFPs are composed of a variable number of peaks depending on the shape of the waveform and the subsequent number of threshold crossings by the one event.

2.2.3. Modify the script to input the electrodes of interest before analysis.

2.2.4. To determine synchronicity (defined in the script by modifiable time frames for synchronous activity to occur within), separate and analyze the extracted latencies to detect coincident events.

NOTE: The script allows the maximum time between coincident events to be set. These are set at 20 ms for EAPs and 200 ms for LFPs.

2.2.5. Run the script to extract latency timestamps.

NOTE: The .xlsx output file contains the interpretations of latency data, which are EAP and LFP counts, frequencies, and coincident event counts for individual electrodes and whole slices. These data are used to assess the frequency, EAP/LFP counts, number of active electrodes, number of coincident events, number of linked electrodes, and the average strength of these linkages.

REPRESENTATIVE RESULTS:

Model of network activity in the spinal cord dorsal horn

Application of 4-AP reliably induces synchronous rhythmic activity in the spinal cord DH. Such activity presents as increased EAPs and LFPs. The later signal is a low-frequency waveform, which has previously been described in MEA recordings[30]. Changes in EAP and/or LFP activity following drug application reflect altered neural activity. Examples of EAPs and LFPs are shown in **Figure 3B** and **Figure 4**. The focus here is on the following parameters or features of the EAP/LFP data: frequency, total counts, active electrode counts, synchronicity as characterized by the number of coincident events detected across multiple electrodes, number of linked adjacent electrodes, and the strength of linkages between adjacent electrodes. Representative results are shown in **Table 3** and **Figure 3, Figure 4, Figure 5, Figure 6, Figure 7,** and **Figure 8**. They show a significant increase in all the parameters measured (all $p<0.001$ by paired *t*-test or the Wilcoxon Signed-Rank non-parametric equivalent test) for both EAPs (**Figure 5** and **Figure 6**) and LFPs (**Figure 7** and **Figure 8**) following 4-AP stimulation and then relative stability for the remainder of the recordings. Data were tested for normality prior to statistical analysis. In summary, 4-AP induces EAP and LFP activity in the spinal cord DH, and various features of the data can be extracted from the MEA recordings. The activity is reproducible, and much of the activity, particularly for LFPs, is rhythmic and synchronous.

[Place **Table 3** + **Figure 4** here]

Slice orientation

The DH circuitry activated by 4-AP is connected in all three dimensions. Thus, slice orientation is an important consideration for *in vitro* preparations. Sagittal or horizontal slicing may be preferential to observe intersegmental signaling, whereas transverse slices better preserve mediolateral and dorsoventral connectivity. Given these considerations, it can be seen that 4-AP stimulation induces similar rhythmic activity in the SDH, regardless of slice orientation (see **Figure 9**).

Long-term stability of 4-AP induced activity

The stability of 4-AP-induced activity is obviously crucial when studying the effects of applied drugs. Therefore, the stability of 4-AP-induced activity parameters was characterized, and this is presented in **Figure 5, Figure 6, Figure 7,** and **Figure 8** and **Table 4**. All activity characteristics, plus the coincidence of activity for LFPs, were stable based on the similarity of 4-AP-induced activity at 12 min after 4-AP application and 15 min later ($p>0.05$). Other LFP synchronicity characteristics, the number of linked adjacent electrodes, and linkage strength between adjacent electrodes decreased over 15 min ($p=0.016$ and $p=0.033$, respectively), though the difference was modest. This gradual change could easily be distinguished from the more immediate actions of a test drug during pharmacological studies (see below). Data were tested for normal distribution before statistical comparisons and then assessed using paired *t*-tests or non-parametric Wilcoxon Signed-Rank tests as appropriate.

[Place **Table 4** here]

Pharmacological investigation of activity characteristics

To demonstrate that MEA-recorded 4-AP-induced activity is readily amenable to pharmacological manipulations, the dependence of these signals on action potential discharge was highlighted. Bath application of the voltage-gated sodium channel antagonist, tetrodotoxin (TTX, 1 μM), abolished both EAP and LFP activity, confirming spike dependency of these signals. Example traces are shown in **Figure 3A.** This result also provides an example of the utility of the preparation for future pharmacological investigations, where novel compounds and established analgesics can be assessed for their action in activated spinal DH circuits. Finally, to shed further light on the relevance of 4-AP activation of the DH networks, an alternative approach was trialed to achieve modest depolarization of the DH network. In this approach, an elevated potassium (4.5 mM) aCSF solution (**Table 1**) was bath-applied and shown to evoke a similar DH response to 4-AP stimulation. This manipulation evoked LFP activity that featured the same synchronous characteristics as 4-AP-induced responses (**Figure 10**), suggesting a similar mechanism and underlying circuitry.

[Place **Figure 5, Figure 6, Figure 7, Figure 8, Figure 9, Figure 10** here]

FIGURE AND TABLE LEGENDS:

Figure 1: Spinal cord slice orientations, mounting and cutting methods. (**A**) Transverse slices require a Styrofoam cutting block with a supporting groove cut into it. The spinal cord is rested against the block in the support groove, the dorsal side of the cord facing away from the block. The block and cord are glued onto a cutting stage with cyanoacrylate adhesive. (**B**) Sagittal slices are prepared by placing a thin line of cyanoacrylate adhesive on the cutting stage and then positioning the spinal cord on its side on the glue. (**C**) Horizontal slices are prepared by placing a thin line of cyanoacrylate adhesive on the cutting stage and then positioning the spinal cord ventral side down on the glue.

Figure 2: Tissue positioning on the microelectrode array. (**A**) Image shows an open MEA headstage with an MEA placed in position. (**B**) Same as **A** with MEA headstage closed for recordings and tissue perfusion system in place. (**C**) Image shows an MEA as supplied by the manufacturer. Contact pads, which interface with the gold springs of the headstage, and the MEA tissue bath that holds the tissue bathing solution and tissue slice are shown. The area highlighted by the red square in the center is the location of the electrode array. (**D**) Schematics show the two MEA electrode configurations used in this study, with further details presented in **Table 2**. The reference electrode is denoted by the blue trapezoid. The left MEA electrode layout shows a 60-electrode square configuration, used most in the presented work—models 60MEA200/30iR-Ti with 30 μm diameter electrodes spaced 200 μm apart, or 200 μm spaced and 100 μm spaced 3-dimensional MEAs (60MEA200/12/50iR-Ti and 60MEA100/12/40iR-Ti) with electrodes 12 μm in diameter and either 50 μm or 40 μm high, respectively. The left MEA electrode layout shows a 6 x 10 electrode rectangular layout—60MEA500/30iR-Ti. (**E**) High-magnification image of a 60MEA100/12/40iR-Ti square MEA with transverse spinal cord slice positioned for recording. The slice sits on electrode rows 3–8. The top row of electrodes, which do not contact any tissue, serve as reference electrodes. The SDH area appears as a semitransparent band. In this case, the SDH overlies electrodes in rows 4, 5, and 6 and columns 2, 3, 4, 5, and 7 of the MEA. Scale bar = 200 μm. Abbreviations: MEA = microelectrode array; SDH = superficial dorsal horn.

Figure 3: Data recording and analysis tool layouts and example microelectrode array recordings showing extracellular action potential and local field potential waveforms. (**A**) Schematic shows preconfigured recording template used for the acquisition of MEA data. Linking the MEA2100 and the recording (headstage/amplifier) tool enables the data to be named and saved. Four example traces of raw data (right, 5-min epochs) were collected by one MEA channel showing activity at baseline, 12 min after 4-AP application, a further 15 min after established 4-AP activity, and following bath application of TTX (1 μM). Note, the addition of 4-AP (second trace) produces a clear increase in background noise and EAP/LFP activity. Importantly, the activity remains relatively stable for at least 15 min after 4-AP-induced activity is established (third trace). Addition of TTX (1 μM) abolishes all activity (bottom trace). (**B**) Schematic (left) shows analyzer software configuration for data analysis. The raw data explorer tool is used to import recordings collected by recording software. These data are then run through a cross-channel filter tool that subtracts the selected reference electrode(s) signal(s) from other electrodes to remove background noise. Data pass through the EAP filter and the LFP filter tools to optimize signal-to-

noise relationships for each waveform. Following this step, the EAP path data enter the EAP detector tool, where thresholds are set. EAPs are detected and then sent to the EAP analyzer tool where the latencies of each event are recorded and exported as a txt. file. An identical workflow occurs for LFP data using a corresponding LFP toolkit. Right traces show data from a single MEA channel containing various extracellular waveforms. Location of EAP and LFP signals are highlighted in the above 'count rasters.' Lower traces are epochs from upper recording (denoted by red bars) showing waveforms on an expanded timescale, including various LFP signals (note the variety of appearances) and individual extracellular EAPs (red circles). Note, LFP/EAP waveform and polarity vary relative to the number of neurons producing these signals, their proximity to the recording electrode, and their location in relation to the nearby electrode(s). Abbreviations: MEA = microelectrode array; EAP = extracellular action potential; LFP = local field potential; 4-AP = 4-aminopyridine; TTX = tetrodotoxin.

Figure 4: Exemplar baseline extracellular action potential activity. Panels show EAP activity (recordings are from different slices). Most electrodes in a given slice recording did not show baseline EAP activity (upper panel). Low-frequency sporadic EAPs were occasionally observed at baseline, potentially containing multiple spike waveforms (middle panel). High-frequency EAP activity was rarely observed in recordings at baseline (lower panel). Insets show individual EAPs from corresponding recordings on an expanded timescale. Abbreviation: EAP = extracellular action potential.

Figure 5: Example 4-aminopyridine-induced extracellular action potential activity. (**A**) Raster plots show EAP activity from active channels, detected at baseline (upper) and two timepoints (12 min – established, and 27 min) following bath addition of 4-AP (middle and lower). Vertical blue windows highlight periods of synchronous (close latency) activity in more than 5 recording electrodes. (**B**) Panels summarize EAP activity map analysis of MEA data. Left schematic shows the orientation of spinal cord slice relative to the electrode array. Middle left panel summarizes activity at baseline (active electrodes colored red) and EAP frequency indicated by white shading around active electrodes (shading intensity denotes increased activity). Middle right panel shows activity in the same slice after 12 min of 4-AP exposure. Note, the number of active electrodes (red) increased along with EAP frequency. In addition, synchrony between adjacent electrodes is indicated by red connecting lines, producing a network map of activity (line thickness denotes the degree of EAP similarity between electrodes). Right panel shows activity in the same slice following a further 15 min of 4-AP exposure. Note the number of active electrodes (red), degree of EAP activity (white), and network structure (red lines) have remained stable over this period. Abbreviations: 4-AP = 4-aminopyridine; EAP = extracellular action potential; MEA = microelectrode array.

Figure 6: Group data summary of 4-aminopyridine-induced extracellular action potential activity. (**A–F**) Group data plots summarizing EAP properties from several experiments identical to the EAP data presented in **Figure 4** (data also summarized in **Table 3** and **Table 4**). EAP frequency (**A**), count (**B**), coincident events (**C**), active electrodes (**D**), linked electrodes (**E**), and average linkage strength (**F**) rose after bath application of 4-AP and were then stable for 15 min following the establishment of 4-AP-induced activity. Data are from 11 experiments (data in red

is from the experiment in **Figure 5**). Abbreviations: 4-AP = 4-aminopyridine; EAP = extracellular action potential.

Figure 7: 4-Aminopyridine-induced local field potential activity. Data are presented as in **Figure 5** except for LFP data. (**A**) Raster plots show LFP activity from multiple channels, detected at baseline (upper) and two timepoints (12 min – established, and 27 min) following bath addition of 4-AP (middle and lower). Vertical blue windows highlight periods of synchronous (close latency) activity in more than 5 recording electrodes. (**B**) Panels summarize LFP activity map analysis of MEA data. Left schematic shows the orientation of spinal cord slice relative to the electrode array. Middle left panel summarizes activity at baseline (active electrodes colored red), with minimal LFP frequency indicated by white shading around active electrodes (shading intensity denotes increased activity). Middle right panel shows activity in the same slice after 12 min of 4-AP exposure. The number of active electrodes (red) and LFP frequency are substantially increased. In addition, synchrony between adjacent electrodes (red connecting lines) shows a strong network map of LFP activity (line thickness denotes the degree of similarity between electrodes). Right panel shows LFP activity in the same slice following a further 15 min of 4-AP exposure. Note the number of active electrodes (red), degree of LFP activity (white), and network structure (red lines) are relatively stable over this period. Abbreviations: 4-AP = 4-aminopyridine; MEA = microelectrode array; LFP = local field potential.

Figure 8: Group data summary of 4-aminopyridine-induced local field potential activity. (**A–F**) Group data plots summarizing LFP properties from several experiments identical to the EAP data presented in **Figure 7** (data also summarized in **Table 3** and **Table 4**). LFP frequency (**A**), count (**B**), coincident events (**C**), and active electrodes (**D**) were stable for 15 min after the 4-AP effect peaked (data in red is from the experiment in **Figure 7**). However, linked electrodes (**E**) and the average LFP linkage strength (**F**) decreased over time (both $p<0.05$). Data are from 11 experiments (data in red is from the experiment in **Figure 7**). Abbreviations: 4-AP = 4-aminopyridine; LFP = local field potential.

Figure 9: 4-Aminopyridine-induced extracellular action potential and local field potential activity in sagittal and horizontal slices. Panels summarize EAP and LFP activity in MEA network map analysis of 4-AP-induced signaling in sagittal (**A**) and horizontal (**B**) spinal cord slices. Schematics (far left) show the orientation of spinal cord slices relative to rectangular electrode arrays. Left network maps show baseline EAP and LFP activity in sagittal (**A**) and horizontal (**B**) spinal cord slices (active electrodes are red, frequency indicated by white shading intensity, and synchrony between adjacent electrodes by red connecting lines with thickness denoting the degree of synchrony). Right network maps show EAP and LFP activity in the same slice after 12 min of 4-AP exposure in sagittal (**A**) and horizontal (**B**) spinal cord slices. Note the substantial increase in the number of active electrodes, frequency of activity, and synchrony of these signals following 4-AP exposure, unmasking networks in both slice orientations. Abbreviations: MEA = microelectrode array; EAP = extracellular action potential; LFP = local field potential; 4-AP = 4-aminopyridine.

Figure 10: Elevated potassium (high K^+)-induced local field potential activity. Panels summarize

high K^+ (4.5 mM) aCSF-induced LFP activity. (**A**) Example traces from one MEA channel at baseline and following bath addition of high K^+ aCSF (5-min epochs). Elevation of K^+ concentration produced clear LFP activity that was absent at baseline, similar to that seen with 4-AP application (**Figure 3**). Inset shows an LFP waveform on an expanded timescale. (**B**) Panels summarize LFP network activity induced by high K^+ aCSF. Left schematic shows orientation of spinal cord slices relative to rectangular electrode arrays. Network maps compare baseline and high K^+-evoked LFP activity (active electrodes red, frequency indicated by white shading intensity, and synchrony between adjacent electrodes by red connecting lines with thickness denoting degree of synchrony). Note the substantial increase in the number of active electrodes, frequency of activity, and synchrony of these signals following high K^+ aCSF exposure, unmasking the underlying network in a similar manner to 4-AP. Abbreviations: aCSF = artificial cerebrospinal fluid; MEA = microelectrode array; EAP = extracellular action potential; LFP = local field potential; 4-AP = 4-aminopyridine.

Table 1: Artificial Cerebrospinal Fluid compositions. Abbreviation: aCSF = artificial cerebrospinal fluid.

Table 2: Microelectrode array layouts.

Table 3: 4-Aminopyridine-induced activity. All presented as means ± SEM.

Table 4: 4-Aminopyridine activity stability. All presented as means ± SEM.

DISCUSSION:

Despite the importance of the spinal DH in nociceptive signaling, processing, and the resulting behavioral and emotional responses that characterize pain, the circuits within this region remain poorly understood. A key challenge in investigating this issue has been the diversity of neuron populations that comprise these circuits[6,31,32]. Recent advances in transgenic technologies, led by optogenetics and chemogenetics, are beginning to unravel these important connections and define the microcircuits that process sensory information[1-4,8-14]. Reconciling how these microcircuits come together to shape activity in larger networks of DH neurons remains challenging, especially for developing new and more effective pain treatments. Here, a functional model of DH activity monitored on MEAs and using 4-AP-stimulated rhythmic activity to study broader network connectivity is described. This model reveals local extracellular spiking (EAPs) and larger network-based LFPs, which depend on action potential discharge and can be used to map changes in network properties. By combining the use of MEAs to facilitate circuit investigation and 4-AP to uncover the underlying circuits, this preparation allows DH circuit function to be studied at a regional or 'macroscopic' level.

Advantages of the MEA/4-AP spinal cord slice model include tight experimental control of an *in vitro* preparation, which is amenable to detailed pharmacological investigation and provides high spatial and temporal resolution of neural activity—individual EAPs and LFPs across a large tissue region and multichannel data—that can assess signaling across networks and regions. Importantly, 4-AP-induced rhythmic activity is reliable, reproducible, and can be studied in

different spinal cord slice orientations. This preparation helps bridge the gap between single-cell and whole-animal investigations and can reveal changes within these circuits under both normal and pathological conditions. The effects of various drugs on network activity can also be determined. Thus, this platform could act as a screening tool for investigating the actions of existing and novel analgesics on DH circuits.

There are several critical steps in this protocol. First, careful tissue preparation is key to producing slices that are viable for experiments and sensitive to 4-AP, regardless of slice orientation. A number of resources are highlighted here that provide detailed information and troubleshooting advice. Briefly, accuracy in making solutions, rapid but meticulous dissection of the spinal cord, optimized slicing parameters to minimize tissue compression and damage, and care when transferring slices at any point are all important factors in the preparation phase. Careful handling of MEAs, particularly when in close proximity to the electrodes, is key to maintaining the function of these components. The optimal position of the DH over the maximum number of MEA electrodes is important for increasing the recording yield of each experiment. When using 3D MEAs, more care and practice are required, especially when positioning and removing slices. It is easy to drag the tissue across protruding MEA electrodes and compromise future use.

There are some caveats to the approach described here. Unlike in single-cell recordings, where the identity of neurons being studied can be determined using either genetic labeling or *post hoc* immunolabeling, the exact source of the electrical signals detected by MEAs cannot be determined. Another challenge is the level of baseline activity in spinal cord slices. Although some reports describe tonically active DH neurons at baseline, the most recent work is in young neonatal tissue[33,34]. Furthermore, tonic activity reported in adult tissue is typically recorded using a searching strategy where electrodes are advanced to first identify and then study this activity[35]. When an unbiased sampling approach is used, establishing recording before assessing activity, less than 20% of adult DH neurons exhibit ongoing spiking (28/150 recordings), and regular discharge was only observed in 2% of these cells (3/150)[36].

Given this ratio and the fixed nature of electrodes relative to a tissue slice, it is unsurprising that few MEA electrodes (~2 electrodes/slice in these MEAs) exhibit activity at baseline. This lack of activity is the primary reason the method described here involves stimulating slices with 4-AP to enhance EAPs and evoked LFP activity. This approach is based on the use of 4-AP to activate rhythmic circuit activity in many *in vitro* preparations, from studying epileptiform mechanisms in the cortex and hippocampus through to fictive locomotor activity in the ventral horn of the spinal cord[37-39]. An extensive literature also highlights that 4-AP induces activity confined to superficial DH circuits in spinal slices and depends on excitatory and inhibitory synaptic transmission as well as electrical synapses [20-22]. Furthermore, *in vivo* 4-AP administration produces a dose-dependent increase in DH neuron receptive fields without altering responses to graded stimulation in the central receptive zone or causing degenerate responses[24]. Finally, it can be seen that a modest depolarization of these circuits by elevating extracellular potassium ion concentration also produces comparable LFP activity. Together, these observations support the view that 4-AP unmasks functionally relevant networks within the superficial DH that can be studied with MEAs. Finally, the exact source of LFP activity is unclear, though these waveforms are thought to

represent a summation of activity detected from multiple neurons surrounding an electrode. They may relate to or result from bursting activity in neurons or correspond to synaptic potentials[30]. Regardless of their origins, the characteristics of LFPs can be compared within and between slices (multiple recordings/drug applications), providing a valuable readout of circuit and network function.

The nature of *in vitro* slice preparations also warrants consideration, with the potential disruption of neuronal circuits and damage to cells on the slice surface. Despite this, slicing the tissue provides more direct electrical access to the relevant DH circuits and uninterrupted pharmacological access. These experimental advantages and disadvantages should be carefully considered, with emphasis on the importance of considering slice orientation to maximally preserve connectivity in the networks of interest. For the vast majority of data presented in this paper, medial-lateral spread of activity within the dorsal horn and the intrinsic connectivity of the neurons in this region are presented. To investigate rostro-caudal activity spread, the use of sagittal or horizontal slices preferentially maintains connectivity between spinal segments, as highlighted in **Figure 9**.

Additionally, it is unavoidable that sectioning the spinal cord will result in some degree of damage at the surface of slices. Minimizing this damage comes back to the careful preparation of tissue, slicing parameters—including slow advance speed and high-frequency blade oscillations—and solutions and conditions that are neuroprotective during this process. A detailed assessment of the benefit of different conditions for spinal cord slice health has been published previously[40]. Notwithstanding the potential impact of slice health on MEA recordings, internal consistency in slice preparation procedures ensures that this factor impacts results across a dataset equally. It should also be noted that that MEA electrodes are thought to pick up signals arising approximately 30–100 µm away from the activity source. As the damaged slice surface is likely to span the top cell layer, approximately 15–30 µm, the effects of slicing-related damage on MEA recordings can be managed and mitigated to still yield valuable datasets and insights on DH network activity[15,41].

In summary, the MEA/4-AP spinal cord slice approach described here provides a platform for understanding the connectivity of DH circuits and how the networks they form drive spinal pain processing. There is also potential for further methodological expansion in terms of analysis parameters, network stimulation source, and its capacity to be used as a platform for pharmacological screening or use with models of pathological pain.

ACKNOWLEDGMENTS:
This work was funded by the National Health and Medical Research Council (NHMRC) of Australia (grants 631000, 1043933, 1144638, and 1184974 to B.A.G. and R.J.C.) and the Hunter Medical Research Institute (grant to B.A.G. and R.J.C.).

DISCLOSURES:
The authors have no conflicts of interest to declare.

REFERENCES:

1 Smith, K. M. et al. Calretinin positive neurons form an excitatory amplifier network in the spinal cord dorsal horn. *eLife.* **8**, e49190 (2019).

2 Smith, K. M. et al. Functional heterogeneity of calretinin-expressing neurons in the mouse superficial dorsal horn: implications for spinal pain processing. *The Journal of physiology.* **593** (19), 4319–4339 (2015).

3 Boyle, K. A. et al. Defining a spinal microcircuit that gates myelinated afferent input: Implications for tactile allodynia. *Cell Reports.* **28** (2), 526–540.e526 (2019).

4 Browne, T. J. et al. Transgenic cross-referencing of inhibitory and excitatory interneuron populations to dissect neuronal heterogeneity in the dorsal horn. *Frontiers in Molecular Neuroscience.* **13**, 32 (2020).

5 Graham, B. A., Hughes, D. I. Rewards, perils and pitfalls of untangling spinal pain circuits. *Current Opinion in Physiology.* **11**, 35–41 (2019).

6 Todd, A. J. Neuronal circuitry for pain processing in the dorsal horn. *Nature Reviews Neuroscience.* **11** (12), 823–836 (2010).

7 Hughes, D. I., Todd, A. J. Central nervous system targets: inhibitory interneurons in the spinal cord. *Neurotherapeutics.* **17** (3), 874–885 (2020).

8 Duan, B. et al. Identification of spinal circuits transmitting and gating mechanical pain. *Cell.* **159** (6), 1417–1432 (2014).

9 Hachisuka, J., Chiang, M. C., Ross, S. E. Itch and neuropathic itch. *Pain.* **159** (3), 603 (2018).

10 Foster, E. et al. Targeted ablation, silencing, and activation establish glycinergic dorsal horn neurons as key components of a spinal gate for pain and itch. *Neuron.* **85** (6), 1289–1304 (2015).

11 Bourane, S. et al. Identification of a spinal circuit for light touch and fine motor control. *Cell.* **160** (3), 503–515 (2015).

12 Cheng, L. et al. Identification of spinal circuits involved in touch-evoked dynamic mechanical pain. *Nature neuroscience.* **20** (6), 804–814 (2017).

13 Peirs, C. et al. Mechanical allodynia circuitry in the dorsal horn is defined by the nature of the injury. *Neuron.* **109** (1), 73–90. e77 (2021).

14 Huang, J. et al. Circuit dissection of the role of somatostatin in itch and pain. *Nature Neuroscience.* **21** (5), 707–716 (2018).

15 Obien, M. E. J., Deligkaris, K., Bullmann, T., Bakkum, D. J., Frey, U. Revealing neuronal function through microelectrode array recordings. *Frontiers in Neuroscience.* **8**, 423 (2015).

16 Nam, Y., Wheeler, B. C. In vitro microelectrode array technology and neural recordings. *Critical Reviews in Biomedical Engineering.* **39** (1), 45–61 (2011).

17 Johnstone, A. F. et al. Microelectrode arrays: a physiologically based neurotoxicity testing platform for the 21st century. *Neurotoxicology.* **31** (4), 331–350 (2010).

18 Stett, A. et al. Biological application of microelectrode arrays in drug discovery and basic research. *Analytical and Bioanalytical Chemistry.* **377** (3), 486–495 (2003).

19 Xu, L. et al. Trends and recent development of the microelectrode arrays (MEAs). *Biosensors and Bioelectronics.* **175** (1), 112854 (2020).

20 Chapman, R. J., Cilia La Corte, P. F., Asghar, A. U. R., King, A. E. Network-based activity induced by 4-aminopyridine in rat dorsal horn in vitro is mediated by both chemical and electrical synapses. *The Journal of Physiology.* **587** (Pt 11), 2499–2510 (2009).

21 Ruscheweyh, R., Sandkühler, J. Epileptiform activity in rat spinal dorsal horn in vitro has common features with neuropathic pain. *Pain.* **105** (1–2), 327–338 (2003).
22 Kay, C. W., Ursu, D., Sher, E., King, A. E. The role of Cx36 and Cx43 in 4-aminopyridine-induced rhythmic activity in the spinal nociceptive dorsal horn: an electrophysiological study in vitro. *Physiological Reports.* **4** (14), e12852 (2016).
23 Jankowska, E., Lundberg, A., Rudomin, P., Sykova, E. Effects of 4-aminopyridine on synaptic transmission in the cat spinal cord. *Brain Research.* **240** (1), 117–129 (1982).
24 Semba, K., Geller, H. M., Egger, M. D. 4-Aminopyridine induces expansion of cutaneous receptive fields of dorsal horn cells. *Brain Research.* **343** (2), 398–402 (1985).
25 Ruscheweyh, R., Sandkühler, J. Long-range oscillatory Ca2+ waves in rat spinal dorsal horn. *European Journal of Neuroscience.* **22** (8), 1967–1976 (2005).
26 Egert, U. et al. A novel organotypic long-term culture of the rat hippocampus on substrate-integrated multielectrode arrays. *Brain Research Protocols.* **2** (4), 229–242 (1998).
27 Thiebaud, P., De Rooij, N., Koudelka-Hep, M., Stoppini, L. Microelectrode arrays for electrophysiological monitoring of hippocampal organotypic slice cultures. *IEEE Transactions on Biomedical Engineering.* **44** (11), 1159–1163 (1997).
28 Rey, H. G., Pedreira, C., Quiroga, R. Q. Past, present and future of spike sorting techniques. *Brain Research Bulletin.* **119**, 106–117 (2015).
29 Satuvuori, E. et al. Measures of spike train synchrony for data with multiple time scales. *Journal of Neuroscience Methods.* **287**, 25–38 (2017).
30 Mendis, G. D. C., Morrisroe, E., Reid, C. A., Halgamuge, S. K., Petrou, S. Use of local field potentials of dissociated cultures grown on multi-electrode arrays for pharmacological assays. In *38th Annual International Conference of the IEEE Engineering in Medicine and Biology Society, EMBC 2016,* 952–956, IEEE (2016).
31 Hughes, D. I. et al. Morphological, neurochemical and electrophysiological features of parvalbumin-expressing cells: a likely source of axo-axonic inputs in the mouse spinal dorsal horn. *The Journal of Physiology.* **590** (16), 3927–3951 (2012).
32 Peirs, C., Seal, R. P. Neural circuits for pain: recent advances and current views. *Science.* **354** (6312), 578–584 (2016).
33 Li, J., Baccei, M. L. Developmental regulation of membrane excitability in rat spinal lamina I projection neurons. *Journal of Neurophysiology.* **107** (10), 2604–2614 (2012).
34 Li, J., Baccei, M. L. Pacemaker neurons within newborn spinal pain circuits. *Journal of Neuroscience.* **31** (24), 9010–9022 (2011).
35 Sandkühler, J., Eblen-Zajjur, A. Identification and characterization of rhythmic nociceptive and non-nociceptive spinal dorsal horn neurons in the rat. *Neuroscience.* **61** (4), 991–1006 (1994).
36 Lucas-Romero, J., Rivera-Arconada, I., Roza, C., Lopez-Garcia, J. A. Origin and classification of spontaneous discharges in mouse superficial dorsal horn neurons. *Scientific Reports.* **8** (1), 9735–9735 (2018).
37 Antonio, L. L. et al. In vitro seizure like events and changes in ionic concentration. *Journal of Neuroscience Methods.* **260**, 33–44 (2016).
38 Avoli, M., Jefferys, J. G. Models of drug-induced epileptiform synchronization in vitro. *Journal of Neuroscience Methods.* **260**, 26–32 (2016).
39 Taccola, G., Nistri, A. Low micromolar concentrations of 4-aminopyridine facilitate fictive locomotion expressed by the rat spinal cord in vitro. *Neuroscience.* **126** (2), 511–520 (2004).

40 Mitra, P., Brownstone, R. M. An in vitro spinal cord slice preparation for recording from lumbar motoneurons of the adult mouse. *Journal of Neurophysiology.* **107** (2), 728–741 (2012).
41 Egert, U., Heck, D., Aertsen, A. Two-dimensional monitoring of spiking networks in acute brain slices. *Experimental Brain Research.* **142** (2), 268–274 (2002).

Figure 1

Click here to access/download;Figure;Figure 1.pdf

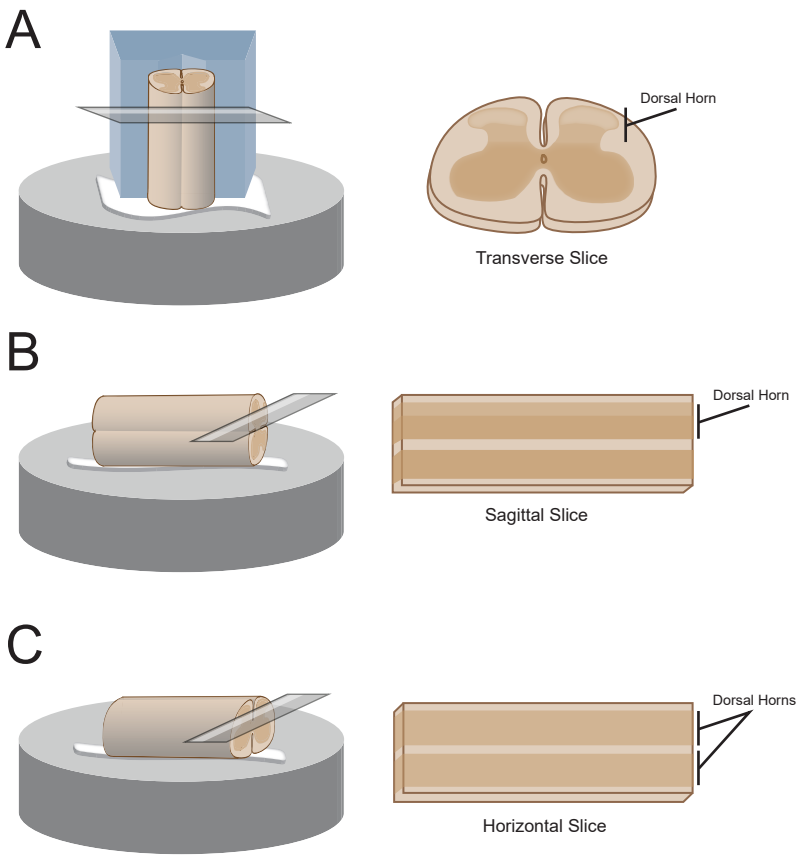

Figure 2

Click here to access/download;Figure;Figure 2.pdf

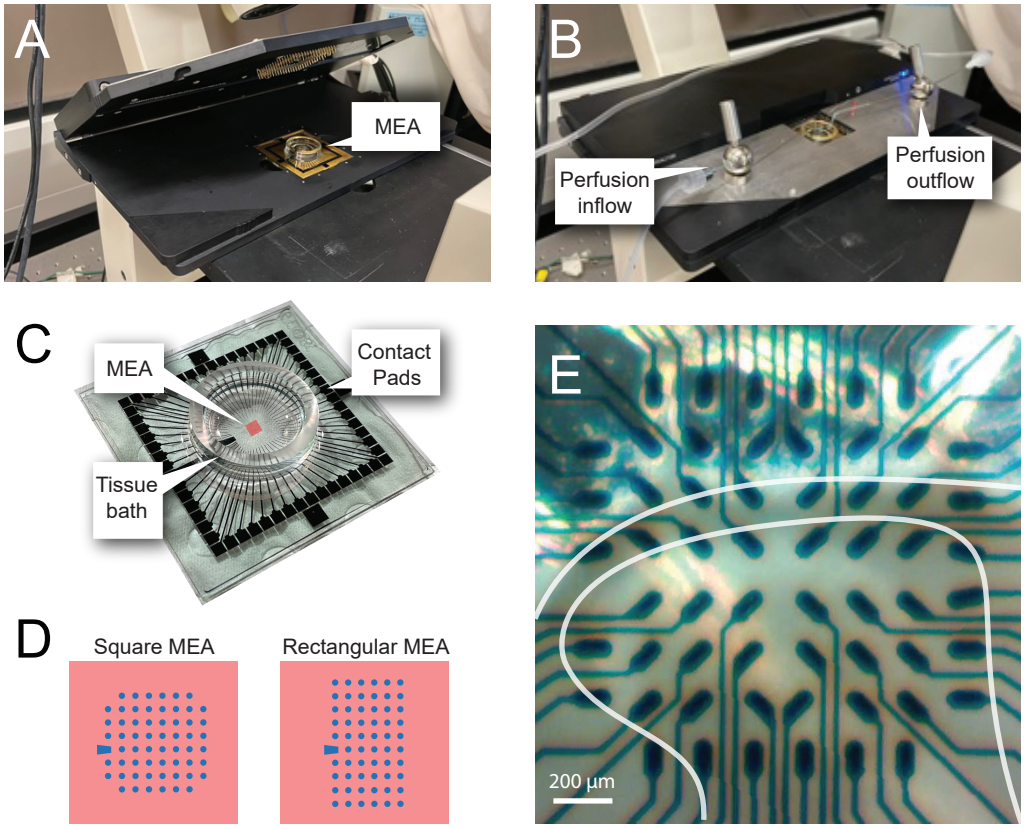

Figure 3

Click here to access/download;Figure;Figure 3.pdf

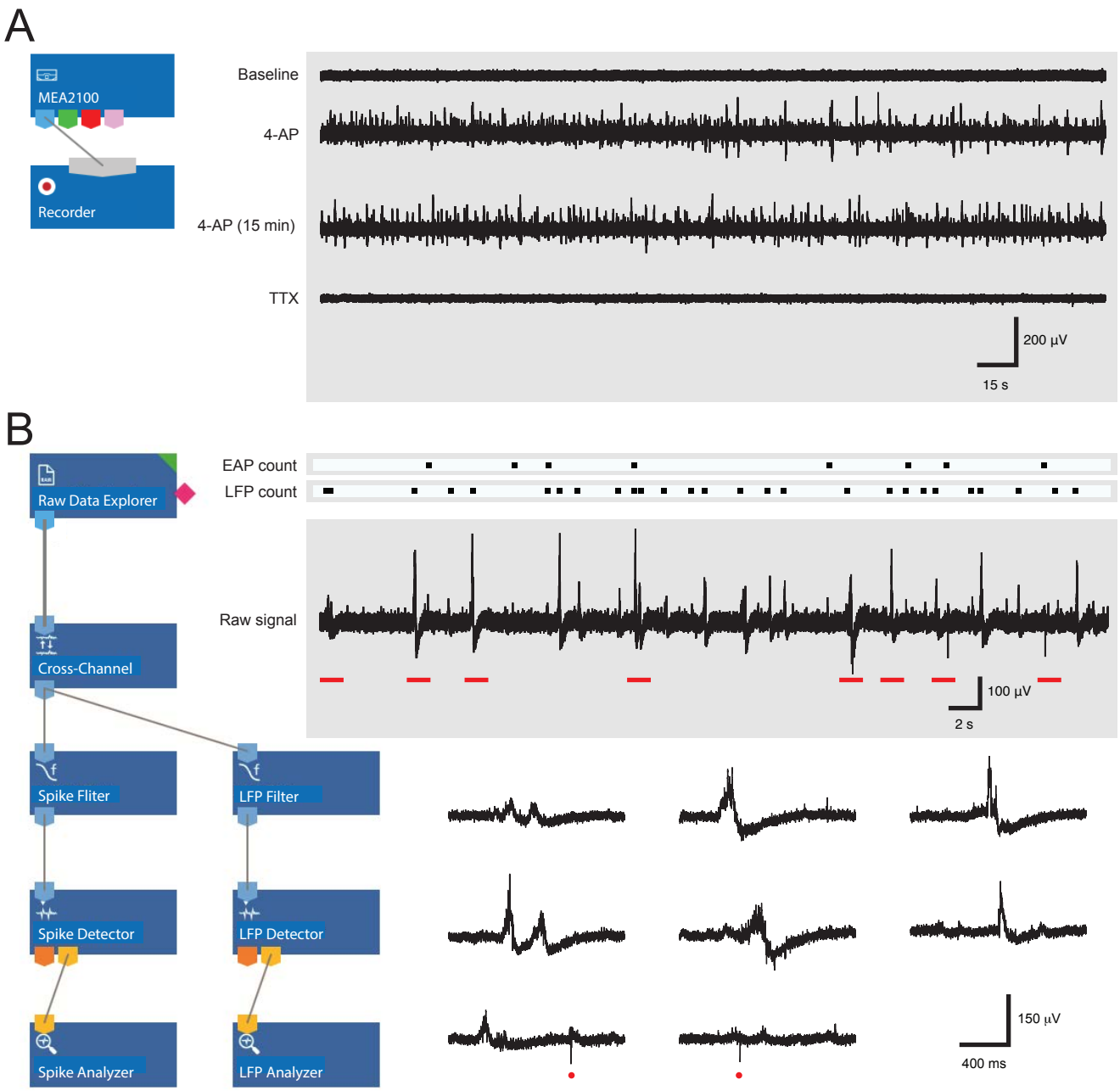

Figure 4

Click here to access/download;Figure;Figure 4.pdf

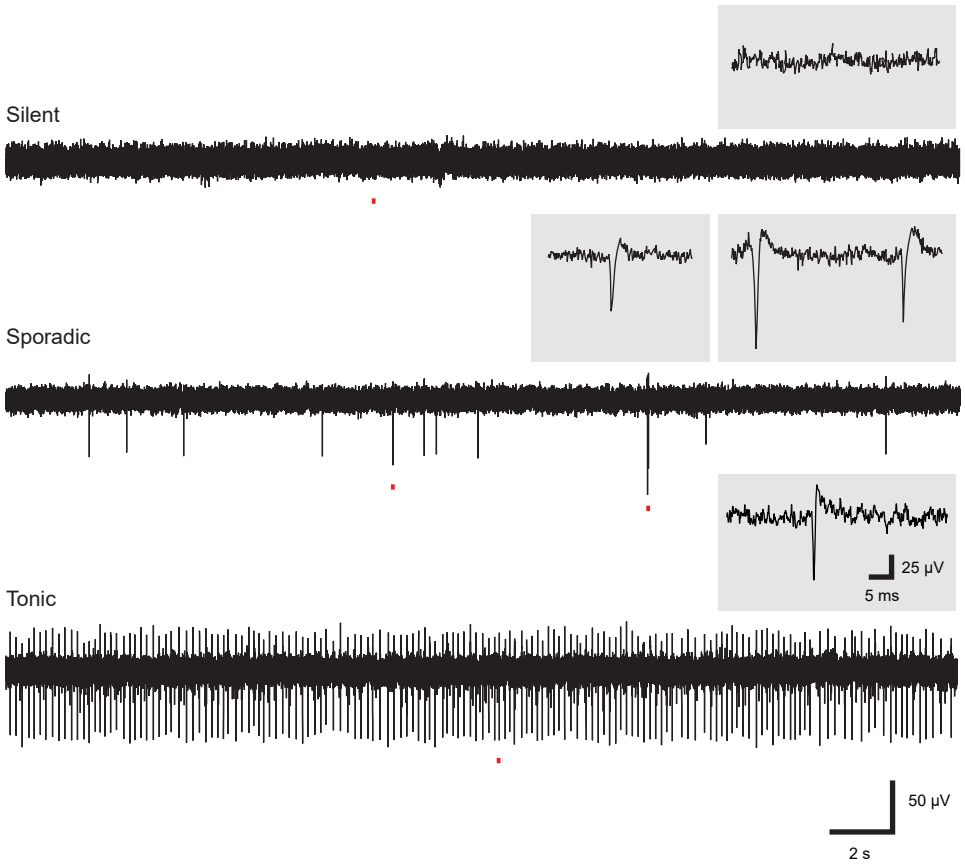

Figure 5

Click here to access/download;Figure;Figure 5 (1).pdf

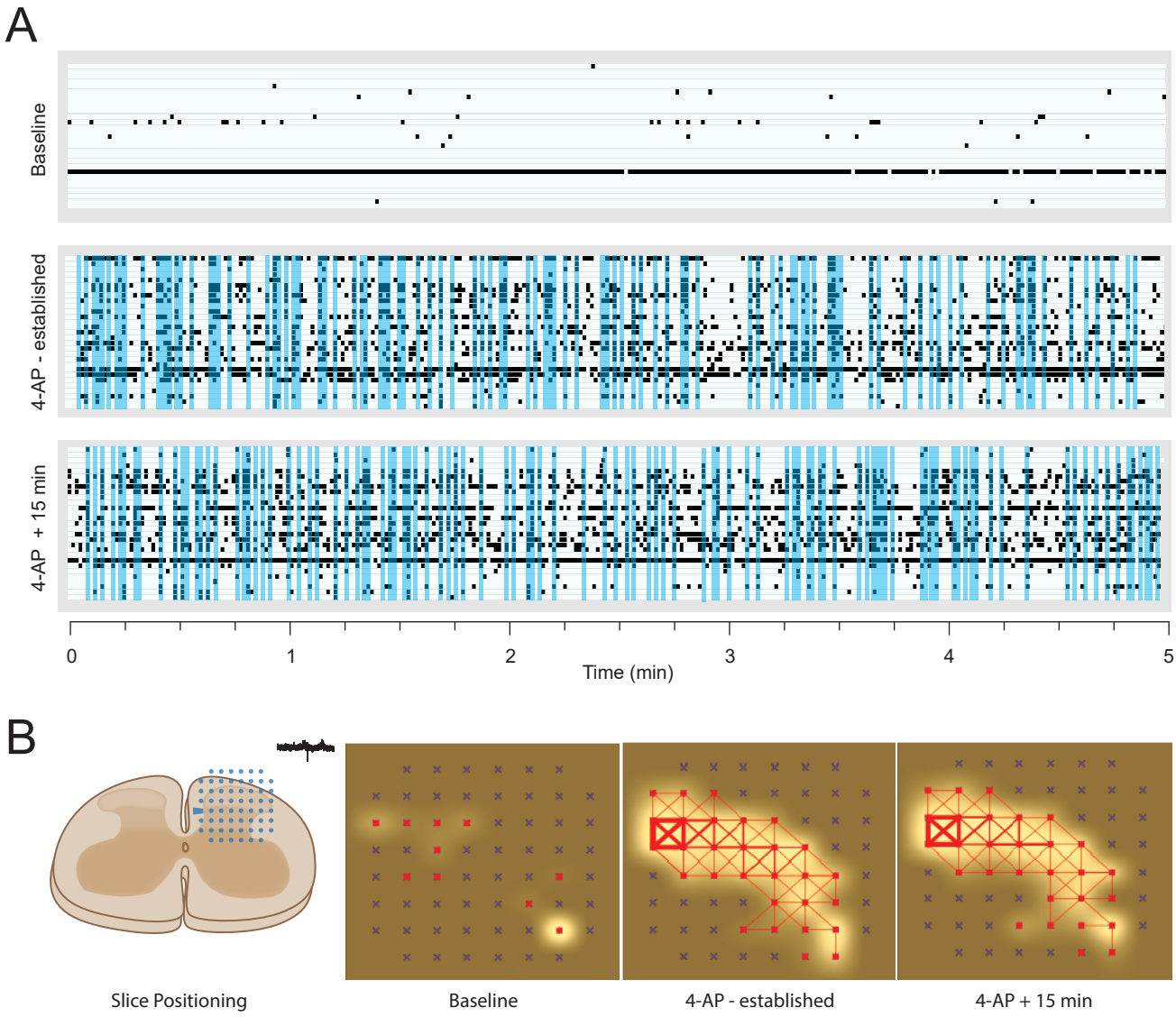

Figure 6

Click here to access/download;Figure;Figure 6.pdf

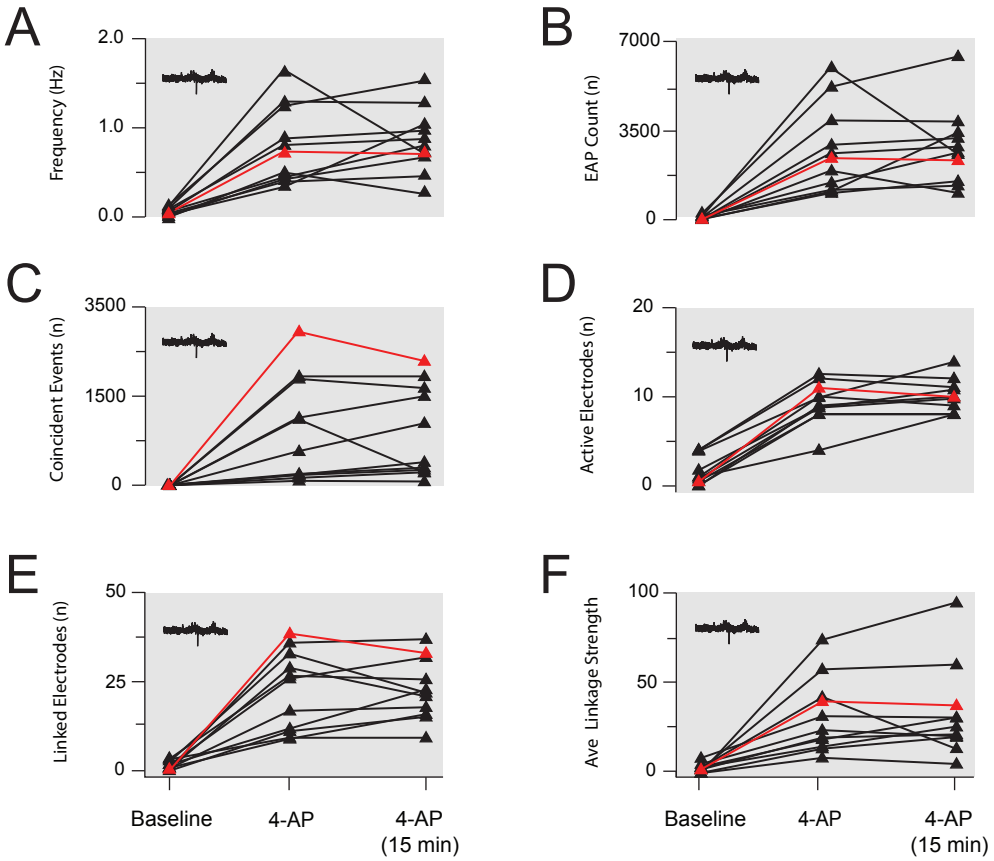

Figure 7

Click here to access/download;Figure;Figure 7.pdf

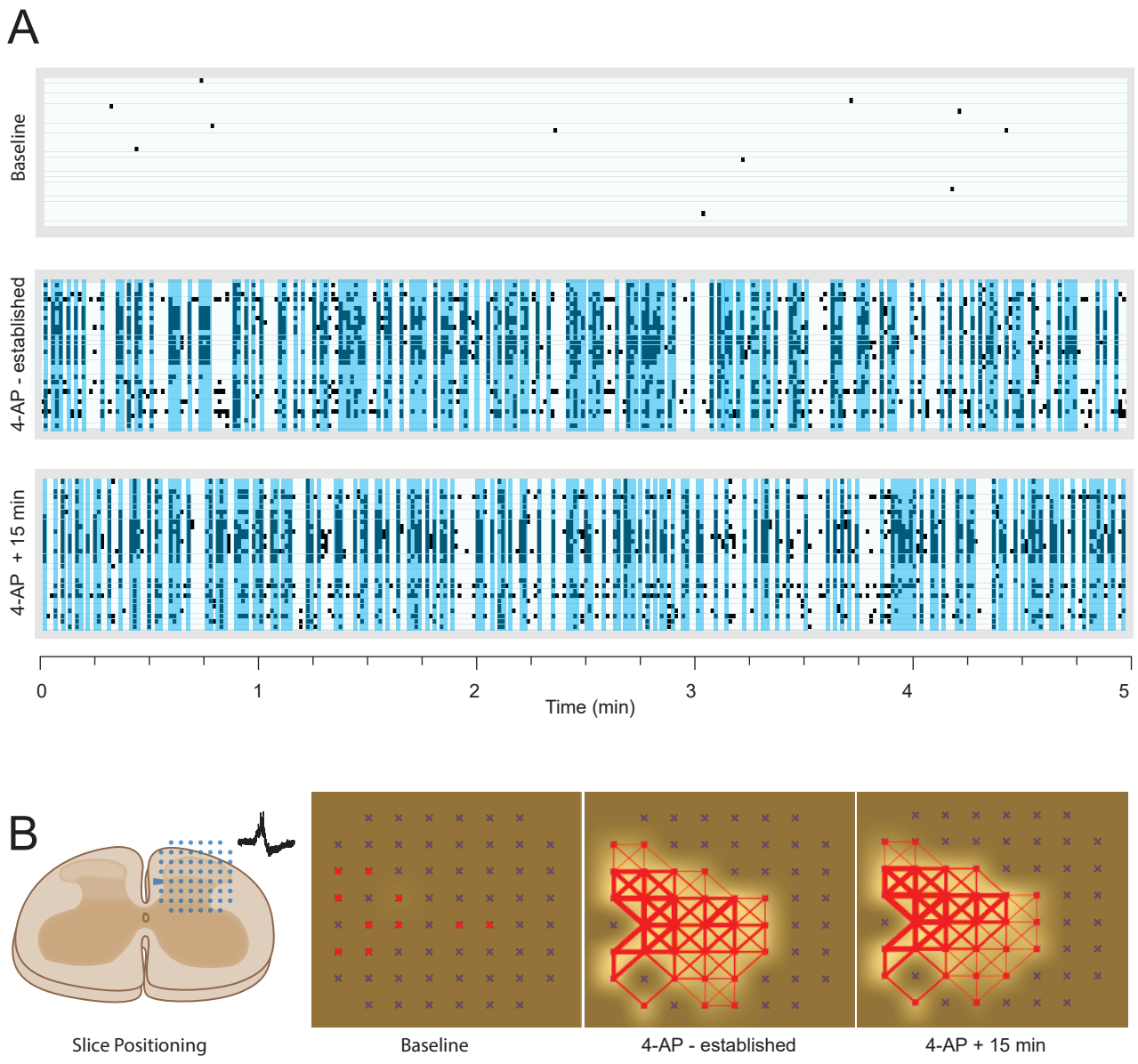

Figure 8

Click here to access/download;Figure;Figure 8.pdf

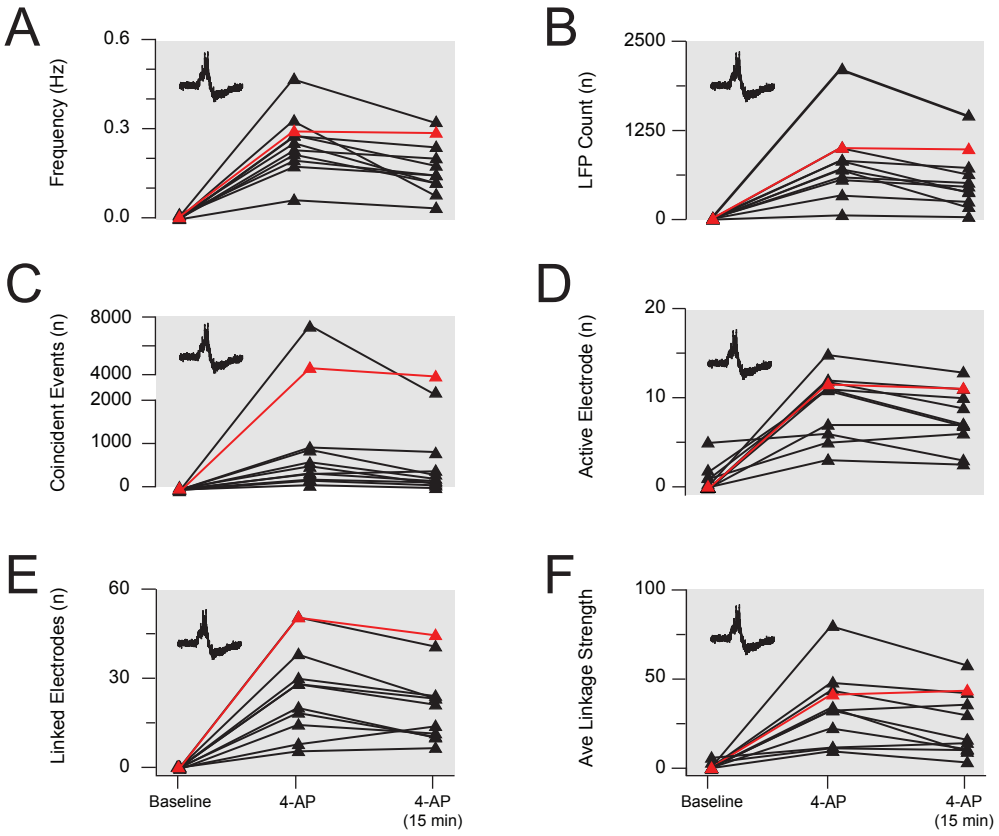

Click here to access/download;Figure;Figure 9.pdf

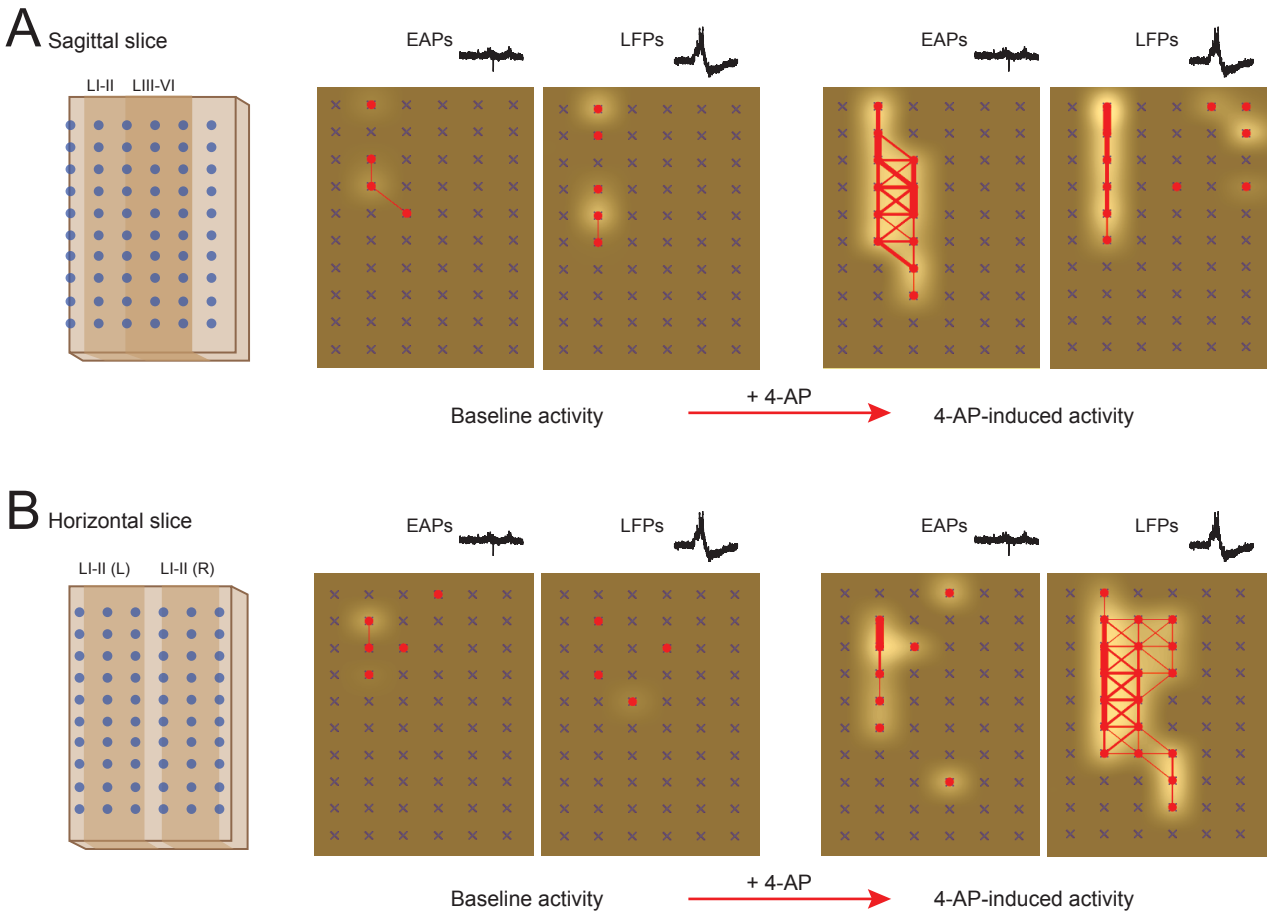

Figure 10

Click here to access/download;Figure;Figure 10.pdf

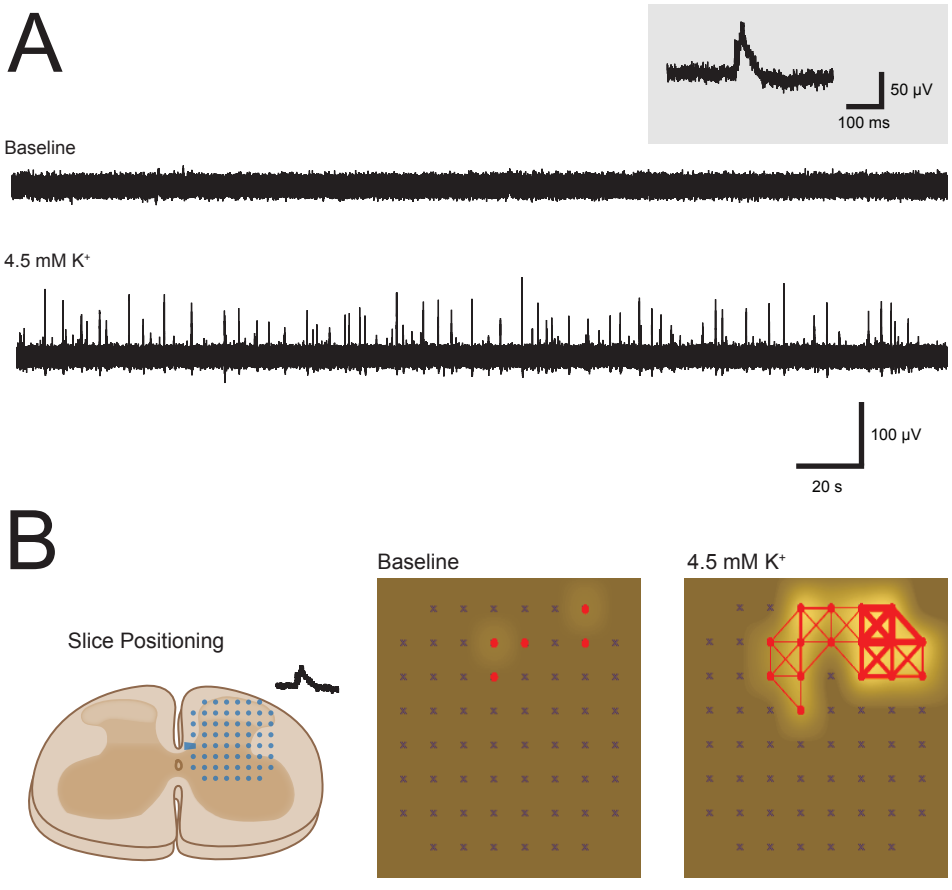

Click here to access/download;Table;Table 1 aCSF Solution Composition Table.xlsx

Table 1.

Chemical	aCSF (mM)	aCSF (g/100 mL)	Sucrose-substituted aCSF (mM)	Sucrose-substituted aCSF (g/100 mL)	High-potassium aCSF (mM)
Sodium chloride (NaCl)	118	0.690	-	-	118
Sodium hydrogen carbonate ($NaHCO_3$)	25	0.210	25	0.210	25
Glucose	10	0.180	10	0.180	10
Potasium chloride (KCl)	2.5	0.019	2.5	0.019	**4.5**
Sodium dihydrogen phosphate (NaH_2PO_4)	1	0.012	1	0.012	1
Magnesium cloride ($MgCl_2$)	1	0.01	1	0.01	1
Calcium chloride ($CaCl_2$)	2.5	0.028	2.5	0.028	2.5
Sucrose	-	-	**250**	**8.558**	-

High-potassium aCSF (g/100 mL)
0.690
0.210
0.180
0.034
0.012
0.01
0.028
-

Click here to access/download;Table;Table 2 MEA Layouts.xlsx

Table 2

Microelectrode Array Layouts				
Microelectrode Array Model	60MEA 200/30iR-Ti	60-3DMEA 100/12/40iR-Ti	60-3DMEA 200/12/50iR-Ti	60MEA 500/30iR-Ti
Planar or 3-Dimensional (3D)	Planar	3D	3D	Planar
Electrode Grid	8 x 8	8 x 8	8 x 8	6 x 10
Electrode Spacing	200 µm	100 µm	200 µm	500 µm
Electrode Diameter	30 µm	12 µm	12 µm	30 µm
Electrode Height (3D)	N/A	40 µm	50 µm	N/A
Experiments	Transverse slice	Transverse slice	Sagittal + Horizontal	Sagittal + Horizontal

Click here to access/download;Table;Table 3 4AP Activity.xlsx

Table 3

Activity Feature	Baseline	4-Aminopyridine	Significant Difference
Extracellular Action Potentials (EAPs)			
Frequency	0.07 ± 0.01	0.88 ± 0.09	p<0.001
Total Spike Count	261.41 ± 70.62	3289. 57 ± 484.38	p<0.001
Active Electrode Count	2.36 ± 0.34	8.95 ± 0.68	p<0.001
Number of Coincident Spikes	9.26 ± 4.01	966.94 ± 189.21	p<0.001
Number of Linked Electrodes	2.03 ± 0.42	24.06 ± 1.96	p<0.001
Strength of Linkages Between Electrodes	1.97 ± 0.58	29.13 ± 4.60	p<0.001
Local Field Potentials (LFPs)			
Frequency	0.00 ± 0.00	0.28 ± 0.03	p<0.001
Total Spike Count	4.79 ± 0.82	688.47 ± 121.16	p<0.001
Active Electrode Count	0.41 ± 0.16	7.64 ± 0.73	p<0.001
Number of Coincident Spikes	0.43 ± 0.23	108.06 ± 278.22	p<0.001
Number of Linked Electrodes	0.24 ± 0.15	22.91 ± 2.46	p<0.001
Strength of Linkages Between Electrodes	0.34 ± 0.19	29.20 ± 3.59	p<0.001

Click here to access/download;Table;Table 4 4AP Stability.xlsx

Table 4

Activity Feature	4-Aminopyridine	4-Aminopyridine (15 min)	Significant Difference
Extracellular Action Potentials (EAPs)			
Frequency	0.8 ± 0.13	0.85 ± 0.10	p>0.05 (no dif.)
Total Spike Count	2706.36 ± 510.96	2838.09 ± 447.73	p>0.05 (no dif.)
Active Electrode Count	9.32 ± 0.70	10.09 ± 0.56	p>0.05 (no dif.)
Number of Coincident Spikes	1037.63 ± 306.84	1013.09 ± 269.80	p>0.05 (no dif.)
Number of Linked Electrodes	22.00 ± 3.37	22.41 ± 2.56	p>0.05 (no dif.)
Strength of Linkages Between Electrodes	30.44 ± 6.27	31.88 ± 7.68	p>0.05 (no dif.)
Local Field Potentials (LFPs)			
Frequency	0.25 ± 0.03	0.17 ± 0.03	p>0.05 (no dif.)
Total Spike Count	792.32 ± 155.83	546.32 ± 120.93	p>0.05 (no dif.)
Active Electrode Count	9.50 ± 1.11	7.86 ± 1.00	p>0.05 (no dif.)
Number of Coincident Spikes	1631.27 ± 734.77	1073.00 ± 490.85	p>0.05 (no dif.)
Number of Linked Electrodes	26.68 ± 4.58	20.95 ± 3.68	p<0.05
Strength of Linkages Between Electrodes	33.35 ± 6.19	24.81 ± 5.41	p<0.05

Click here to access/download
Table of Materials
JoVE_Materials (2).xlsx

Rebuttal Letter
Click here to access/download;Rebuttal Letter;Iredale et al 2021 Reviewer responses v2.docx

RESPONSE TO REVIEWS

JoVE editors and reviewers, we appreciate the opportunity to address the feedback provided on our submission and believe the process has further improved our manuscript. Below we provide a detailed a point-by-point response to this input with amendments highlighted by red text in our manuscript. This revision has addressed all reviewer and editors comments as requested.

Editorial Comments

Point 1) Please take this opportunity to thoroughly proofread the manuscript to ensure that there are no spelling or grammar issues. Please define all abbreviations at first use.
Response: Manuscript thoroughly read with all identified spelling, grammar and abbreviation issues addressed.

Point 2) Please consider providing reaction set-ups and solution composition as Tables in separate .xls or .xlsx files uploaded to your Editorial Manager account. These tables can then be referenced in the protocol text.
Response: Solution composition tables uploaded to editorial manager account and referenced in protocol text. *See page 4, lines 141, 143, 157, and page 12 lines 498 and 508; and new Table 1.*

Point 3) JoVE cannot publish manuscripts containing commercial language. This includes trademark symbols (™), registered symbols (®), and company names before an instrument or reagent. Please remove all commercial language from your manuscript and use generic terms instead. All commercial products should be sufficiently referenced in the Table of Materials and Reagents.
Response: All commercial language removed for manuscript and figure legends and commercial products only referred to in table of materials and reagents.

Point 4) Please revise the text, especially in the protocol, to avoid the use of any personal pronouns.
Response: Text revised, and all personal pronouns removed.

Point 5) Please ensure that all text in the protocol section is written in the imperative tense.
Response: Text revised and where required changed to imperative tense.

Point 6) Please note that your protocol will be used to generate the script for the video and must contain everything that you would like shown in the video. Please ensure you answer the “how” question, i.e., how is the step performed? Alternatively, add references to published material specifying how to perform the protocol action. There should be enough detail in each step to supplement the actions seen in the video so that viewers can easily replicate the protocol.
Response: Text revised and where needed clarification on how the step should be performed was made more direct.

Point 7) Please format the manuscript as: paragraph Indentation: 0 for both left and right and special: none, Line spacings: single. Please include a single line space between each step, substep and note in the protocol section. Please use Calibri 12 points and one-inch margins on all the side. Please include a ONE LINE SPACE between each protocol step and then HIGHLIGHT up to 3 pages of protocol text for inclusion in the protocol section of the video.
Response: Text revised and formatted according to guidelines.

Point 8) Please add limitations of the technique to the discussion.
Response: More extensive treatment of limitations added to discussion. *See page 16, 17 and 18, lines 689-701, 706-708 and 716-736.*

Point 9) Do not abbreviate journal titles
Response: Text revised, and journal title abbreviations removed.

REVIEWER #1
Major Concerns

Point 1) While the notion of a neuropharmacological assay where spontaneous activity driven by K channel inhibition may have some utility, it is not clear whether or not other compounds typically used to promote rhythmic firing (GABA_A receptor blockers) might have a similar effect.
Response: Our decision to use 4-AP to induce spontaneous activity in the dorsal horn of spinal slices is now more clearly justified, while also acknowledging that alternative methods have also been used in various CNS regions. We now cite this literature, which includes chemically induced rhythmic epileptiform behaviour in brain slices, and fictive locomotor behaviour in the ventral horn of the spinal cord. We also justify our choice of 4-AP as it has been used in several dorsal horn studies and been assessed pharmacologically, including its sensitivity to a range of antiepileptics and analgesics. Finally, we now show that modifying potassium ion concentration can also induce a similar pattern of spontaneous activity, providing a complementary ionic approach to drug mediated induction of activity. *See page 3, lines 107-115; page 12; lines 491-497; page17, lines 697-701; and Figure 10.*

Point 2) The claim that the assay could support the discovery of antinociceptive compounds is not compelling since TTX is far from a compelling model. Why not lidocaine or carbamazepine?
Response: Application of TTX in our manuscript is used to simply highlight the preparation is amenable to pharmacological studies, while at the same time confirming that rhythmic LFP activity is a network signal that is dependent on spiking. Justification for use of 4-AP to assess antinociceptive compounds is now better supported citing previous patch clamp work that screened the effects of both analgesics and antiepileptic drugs on 4-AP induced activity in dorsal horn neurons. These results suggested that drug sensitivity of the 4-AP assay was similar to the pharmacological profile in neuropathic pain patients. Finally, we note the JoVE does not require experimental data comparisons and thus a more detailed pharmacological screen was not undertaken. *See page 3, lines 107-115.*

Point 3) How long can the slices be maintained acutely? If it is only 15 min, this is far from long-term stability such that the utility as described is highly limited.
Response: Apologies for the misunderstanding. Following preparation, spinal cord slices can be maintained for approximately 6 hours in the incubator. Once a recording begins and 4-AP applied, we confirmed that rhythmic activity is maintained for at least 15 minutes. This was considered sufficient time for an *in vitro* drug assay, allowing 4-AP induced activity to be assessed prior to and following drug application. The average duration that spinal cord slices remain viable, and clarification of how long stable 4-AP induced activity was assessed, are now more clearly described in our revision.

REVIEWER #2
Major Concerns
Point 1) An important issue is related to the lack of rhythmic activity showed by the authors under control conditions, their interpretation and the use of 4-AP. There are several works that have shown spontaneous spiking activity and intrinsic rhythmicity in the spinal cord under in vivo conditions (Pain. 1976 Mar;2(1):5-24. doi: 10.1016/0304-3959(76)90042-7, Neuroscience. 1994 Aug;61(4):991-1006. doi: 10.1016/0306-4522(94)90419-7), and hence spontaneously active neurons are likely present in the spinal cord under physiological conditions. In spinal cord preparations in vitro, there are also works that had reported considerable rhythmic activity (J Neurosci. 2011 Jun 15;31(24):9010-22. doi: 10.1523/JNEUROSCI.6555-10.2011; J Physiol. 2014 Apr 1;592(7):1519-34. doi: 10.1113/jphysiol.2013.269472). Although the proportion of neurons with rhythmic activity can be low, the use of multiple electrodes must facilitate the recording of spontaneously active neurons and enable its study. This seems to be successfully done using a similar slice approach and multielectrode arrays (Sci Rep. 2018 Jun 27;8(1):9735. doi: 10.1038/s41598-018-27993-y; Pflugers Arch. 2016 Nov;468(11-12):2017-2030. doi: 10.1007/s00424-016-1886-6). Its appears that the age of the animals in these in vitro studies was lower than in the present ms (3-12 months here vs animals under 2 months), and that the proportion of spontaneously active neurons may decrease with age (J Neurosci. 2011 Jun 15;31(24):9010-22. doi: 10.1523/JNEUROSCI.6555-10.2011). However seems difficult to justify an impossibility to work with non-pharmacologically-induced rhythmic activity only by the age of the animals.
Response: These points are now clarified in the manuscript. Of course we don't dispute that some cells are spontaneously active (and sometimes rhythmically) in the dorsal horn. The work referred to is now cited, with the caveat that studies reporting such activity are predominantly limited to young neonatal tissue. We have also added note of literature on spontaneous activity in the spinal cord of adult animals. Importantly, this work is done using a search strategy where electrodes are advanced

into tissue to identify active cells, a very different approach to the static sampling that is achieved when a slice is placed on a fixed array of electrodes. In fact, the examples provided by the reviewer of spontaneous activity (Sci Rep. 2018 Jun 27;8(1):9735. doi: 10.1038/s41598-018-27993-y; Pflugers Arch. 2016 Nov;468(11-12):2017-2030. doi: 10.1007/s00424-016-1886-6) use single shaft MEAs that are advanced through the preparation until activity is detected. Furthermore, this work reports very low levels of activity when patch clamp recording, which does not afford a prospective search for active cells, is used. This detail is now added to the manuscript and is consistent with our report of low baseline activity levels and use of an approach (4-AP stimulation) to enhance activity in the slice and unmask regional networks. *See page 16 and 17, lines 689-701.*

Point 2) The slicing procedure made can be affecting the results obtained. First, it is likely that the portions close to the cut border have been damaged by the blade, and hence may have low functionality. Although the authors used 3D electrodes these have a low size and may still be located in a partially damaged portion. Second, as slices seem to be cut in both sides, this could have severed many connections reducing the active contacts within the circuits. This is also important given the claim of the authors that this approach may be useful for studying spinal circuits' activity.
Response: It is certainly widely accepted by slice electrophysiologists that some level of cell damage occurs at the cut surface of slices. This has not hampered the field from making substantial progress in mapping dorsal horn circuits, including the use of optogenetics. Furthermore, the same method is used for every experiment which enables consistency in data collection and any damage related impact is unlikely to skew results. It should be noted that previous work suggests MEA electrodes pick up signals from approximately 30-100 µm away from the activity source, conversely it is estimated that cell damage on the cut slice surface spans approximately 15-30 µm. Together, these parameters support the utility of the preparation as described in our manuscript. Importantly, we also highlight the potential to make recordings from multiple slice orientations, accounting for the orientation of DH circuits. These consideration and caveats are now added to our expanded discussion. *See page 16 and 17, lines 716-736.*

Point 3: The use of 4-AP inevitably alters the operation of spinal circuits and reduce the relevance of the data obtained. In a methodological ms like this, I consider that at least a discussion of these issues (if the authors do not find an experimental way to deal with them), together with sufficient and unbiased citation of the literature may give the reader a complete vision of the possibilities of this procedure and additional alternatives that may enhance its applicability.
Response: Literature describing the background and existing understanding of 4-AP induced activity in the dorsal horn was cited in our original manuscript (i.e., studied using patch clamp, extracellular recording and calcium imaging; requires intact excitatory and inhibitory synaptic transmission; expands receptive fields when applied in vivo). Nevertheless, and expanded treatment of this literature is now included in our revision. We also note that other pharmacological and ionic strategies can be used to evoke spontaneous activity in slice preparations. Much of this literature is developed in the field of epilepsy using brain slices, though similar strategies are also used to induce fictive locomotor activity in the ventral spinal cord. This work is now cited, but we also take the opportunity to emphasise that use of 4-AP to induce activity in the dorsal horn has the greatest evidence and background information. In addition, we have added data showing that modest elevation of potassium concentration in the bathing (aCSF) solution can also evoke rhythmic activity with the same characteristics as 4-AP. This reinforces the utility and biological relevance of the methodology described in our manuscript. *See page 3, lines 107-115; page 12; lines 491-497; page17, lines 697-701; and Figure 10.*

Point 4: The use of slices with attached roots will also increase the options for these studies. This may enable the activation of primary afferent terminals to activate intrinsic circuits and neurons, perhaps avoiding the pharmacological intervention with 4-AP.
Response: There are many methods descriptions that detail preparation of dorsal root attached slice preparation, including our own. This is outside our intended scope, and we therefore simply acknowledge that this alternative would be possible.

Point 5: It is quite surprising that the authors do not shown any example of an extracellular action potential in which was possible to judge the quality of the recording. In figures 3B, 4A and 5 there are some fragments of the recording in a time scale that impedes to identify the characteristics of the action potential. Considering the analysis itself, it is currently more common to analyse extracellular recordings using spike sorting than simply a threshold-based criterion. There are multiple possibilities

of analysis programs (some of them free access) that can be used in order to classify the recorded activity and obtain more precise information from the experiments. Have the authors tried to perform this type of analysis? This also may help to obtain a more accurate analysis, since it seems strange to read "less than 10 EAPs should be detected in reference electrodes where physiological activity won't be occurring", and such activity will probably be excluded with an adequate analysis.
Response: We now provide a new figure that shows a series of recordings spanning the range of extracellular action potential activity, as well as examples on an expanded timescale to show the quality of obtained recordings. We also add a note to highlight our pooling of extracellular action potentials as a single population for each electrode, and a reference a detailed review of spike sorting strategies and analysis for readers that wish to pursue this analysis. *See page 9, lines 370-374; page 10; lines 396-403; and Figure 4.*

Point 6: To study synchronicity, the authors indicate that they have used a method described in a previous work from Satuvuori, et al. However, I'm not sure if they use the same tool or an adapted version, this need to be clarified, and also if this tool is available or not, and where get it, if it was possible.
Response: We used equations published in the Satuvuori, et al. paper to undertake our synchronicity analysis, not a method or tool. These details are available in section 2.3 of the Satuvuori, et al. paper, equation 20, for readers that wish to access this information.

Minor Concerns
Point 1) It seems for the examples in figs 4B and 6B that EAPs and LFPs in the presence of 4-AP may occur in slightly different areas of the cord, LFPs in deeper regions. Have the authors seen any relation between the type of activity elicited and the area of the cord?
Response: Data presented in figures 4B and 6B is example data from two different slices leading to the difference in location. The schematic of MEA electrode location under the DH, shown in panel B on the left for both figures, is an estimate location and subsequently the difference in activity partially stems from the DHs of each slice sitting in a slightly different location on the MEA. Additionally, the area of activity does differ between slices, however, no obvious pattern of difference is evident between activity types, and this has not been investigated further.

Point 2) Looking at figure 8B it seems that there is more synchronization between left and right sides than inside the right side, is this possible?
Response: Figure 8B shows activity recorded in a horizontal slice. Activity is predominantly in the left dorsal horn as shown by the thicker connecting lines. Some activity is also resolved in the right side, though much less than left. Coincident activity between side is possible, although many other factors such as slice depth and subtle off axis orientations could contribute. This is not a significant feature in the data.

Point 3) In section 1.1.2 indicate that sucrose aCSF was introduced in a -80ºC freezer, but then in section 1.3 seems that "ice-cooled" aCSF was used. At first glance, -80ºC seems a rather low and perhaps uncommon temperature for living tissues, that could affect the viability of the preparation. Please explain and justify if necessary.
Response: The -80ºC freezer was used to freeze the solution to an ice-cold consistency quickly. The temperature of the solution when used to cool the tissue was below 0º but much higher than -80ºC as the solution was removed from the freezer, vigorously shaken and stirred to achieve a ‘slurry’ consistency and held at room temperature prior to use. This is now clarified in the text. *See page 4, line 166.*

Point 4) Although the authors used carbanox, perhaps other 95% O2, 5% CO2 gas mixtures could also be adequate and easier to obtain?.
Response: Carbanox is simply one trade name for the common 95% O2, 5% CO2 gas mixture used in electrophysiological procedures across the literature, also referred to as Carbogen. We now clarify this and refer to the gas mixture by composition.

Point 5) In Fig 1, sagittal slice picture shows a line of white matter in the centre that may not correspond to the position indicated with the blade.
Response: This image depicts a lateral sagittal slice where the lateral fasciculus is interposed between the dorsal and ventral horns. We can confirm that the depiction is accurate with several years of experience preparing this tissue.

Point 6) In figure 2E it is difficult to appreciate the borders of the cord and the semi-transparent band that correspond to SDH.
Response: This image is a realistic reflection of the likely appearance of the preparation. Superimposed outlines highlight the spinal cord slice positioning. We believe this gives the reader sufficient landmarks to correctly orient the tissue on an MEA.

Point 7) Raster plots in figures 4A and 6A. How were these graphs constructed? Is each row a different channel? How are ordered the channels? Only "active" channels are included? How can be compared the same channel under different conditions using this graph? Are the bins 1 second long?
Response: In terms of the construction of the raster plots, each channel represents a different electrode, and the bins are 1 second long. Previously only active channels were shown, however, to clarify confusion previously excluded inactive channels have now been included. This means channels now correspond between conditions, i.e. channel 1 in baseline corresponds to channel 1 in 4-AP and 4-AP 15 minutes. *See Figures 5 and 7.*

Point 8) The authors must indicate the parameters used for slicing. Although is likely that the parameters must be adjusted for each vibratome, an indication will be useful for other researchers.
Response: Details on the vibratome settings have been added to the manuscript. *See page 6, lines 242-243.*

Point 9) Please correct line 469 (traces are at the right), and line 484 (in).
Response: Corrected.

REVIEWER #3
Point 1) There is a mention about a MATLAB script, but the code is not given.
Response: MATLAB script now included in manuscript. We note that provision of this code necessitated a new author (Augustus Elton) be added to our manuscript. Author details are updated accordingly.

Point 2) Replace excel with Excel.
Response: All mentions of Excel have been removed at the editor's request (no commercial language should be used in the manuscript).

Click here to access/download
Supplemental Coding Files
JoVE Code.zip